ACS OMEGA

Open Access

http://pubs.acs.org/journal/acsodf

Article

Investigation of Weak Noncovalent Interactions Directed by the Amino Substituent of Pyrido- and Pyrimido-[1,2-*a*]benzimidazole-8,9-diones

Anastasija Gaile, Sergey Belyakov, Vitālijs Rjabovs, Igors Mihailovs, Baiba Turovska, and Nelli Batenko*

Cite This: *ACS Omega* 2023, 8, 40960−40971

Read Online

ACCESS | Metrics & More | Article Recommendations | Supporting Information

ABSTRACT: Quinones are small redox-active molecules that are able to form intra- and intermolecular interactions both in the solid state and in solution. On the basis of 6-amino-substituted pyrido- and pyrimido-[1,2-*a*]benzimidazole-8,9-diones, weak interactions were investigated by single-crystal X-ray and ^{1}H NMR spectroscopy methods. Crystallization of quinone derivatives containing a −NH−CH_2− fragment led to the formation of both chiral and achiral crystals. The presence of two forms with (*endo* form) and without (*exo* form) an intramolecular hydrogen bond was experimentally detected by X-ray crystallography analysis and variable-temperature (VT) ^{1}H NMR experiments in the cases of *iso*pentylamino- and benzylamino-substituted derivatives. Interestingly, the *exo* form dominates both in the solid state and in solution.

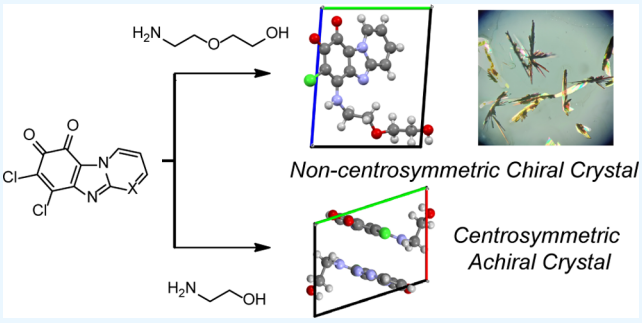

INTRODUCTION

Quinones and quinone derivatives are small molecules involved in numerous significant biological processes such as photosynthesis,[1] cellular respiration,[2] intra- and extracellular signaling,[3] and metabolic transformations with cytotoxic or cytoprotective effects.[4] Quinones are used as cocatalysts in palladium catalysis[5] and electron-transfer mediators in metal catalyzed reactions,[6] as well as redox reservoirs in water electrolysis processes.[7] Promising results were achieved for the application of quinone derivatives as quinone electrode materials[8,9] for Li−organic batteries,[10,11] zinc−organic[12] batteries, and metal-free symmetric quinone-acid cells.[13]

It is known[14] that the relatively weak intra- and intermolecular interactions influence different physicochemical properties such as the melting/boiling point, the solubility, the morphologies, and the charge transport in organic materials. As quinones are conjugated cyclic diketones, their carbonyl groups can form hydrogen bonds (H-bonds) with different groups (e.g., −OH or $-NH_2$). As a result, stabilization of the supramolecular structure of quinone derivatives by a network of synergistic noncovalent forces (H-bonding and $\pi-\pi$ stacking) was observed.[10,11,15] For example, thermal stability and low solubility of 2,5-diamino-1,4-benzoquinone[10] in battery electrolytes were demonstrated and explained by the formation of a H-bond between amino and carbonyl groups polarized by electronic delocalization. Another example is a stabilization of the supramolecular structure of 2,3-diamino-7,8-dihydroxyphenazine-1,4-dione[11] by intermolecular interactions and $\pi-\pi$ stacking. The rational design of quinone derivatives can be used for the construction of ordered redox-active molecular solids.[16] It was demonstrated[17,18] that crystallization and supramolecular assembly can be controlled by the combination of different inter- and intramolecular interactions, but the use of such a control is still a complex problem.

It was reported[19] that quinones with replaceable halide substituents react with amines, amino alcohols, and amino acids: the formation of a carbon−nitrogen bond does not produce a new chirality center as it proceeds via an addition/elimination sequence. Conformationally flexible fragments with proton-donating abilities may allow the stabilization of different modes of H-bonds[20] that in turn can affect the formation of supramolecular systems as well as physical properties of the resulting compounds. The development of a generalized data set of substituents with the ability to form multiple H-bonds in the solid state as well as in solution is essential. Therefore, there remains a demand to establish possible weak intra- and intermolecular interactions of quinone derivatives because understanding such interactions can provide a useful approach to designing new materials in general and crystal engineering in particular.[21]

Received: September 13, 2023
Accepted: September 26, 2023
Published: October 19, 2023

https://doi.org/10.1021/acsomega.3c07005
ACS Omega 2023, 8, 40960−40971

We selected pyrido- and pyrimido-[1,2-*a*]benzimidazole-8,9-diones for the investigation of the formation of intra- and intermolecular interactions upon modification of the initial core with amines and amino alcohols. Initial compounds (**1a,b**) contain a combination of *o*-quinone and imidazo[1,2-*a*]pyridine (H-bond acceptor) fragments. Imidazo[1,2-*a*]-pyridine derivatives tend to form intramolecular H-bonds between the substituent and nitrogen of the heterocycle.[22] It was observed that derivatives of pyrido- and pyrimido[1,2-*a*]benzimidazole-8,9-dione (Scheme 1a) possessing an electron-withdrawing group at the C(6) position can form H-bonded dimers[23] as well as $\pi-\pi$ stacking interactions in the solid state.[24]

Scheme 1. (a) Synthesis of Compounds 3a−g and 4a,b (Compounds 3d,e Were Isolated as Hydrochloride Salts); (b) Mesomeric Forms of Derivatives 3a−g and 4a,b

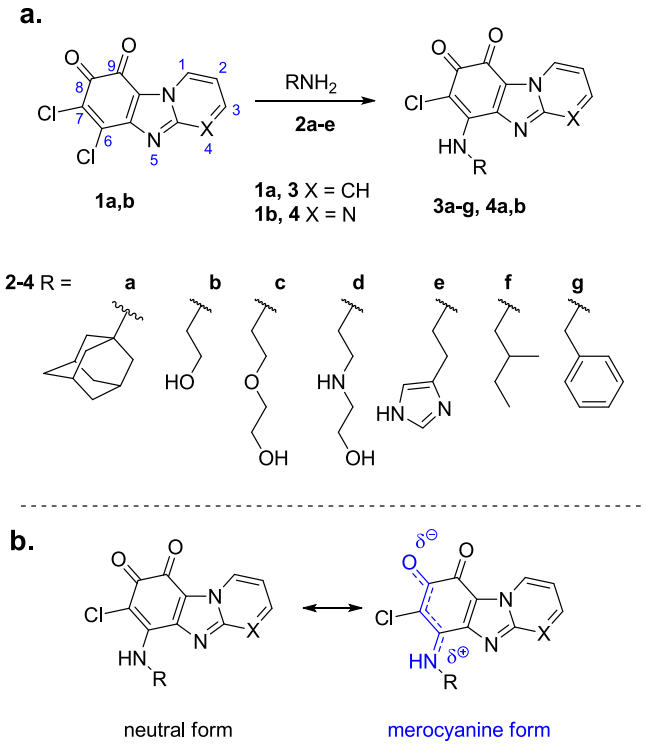

RESULTS AND DISCUSSION

Synthesis. In this work, quinone derivatives **3a−g** and **4a,b** were obtained via a simple one-step nucleophilic substitution reaction using different amines **2a,e−g**, aminoethanol (**2b**), and its elongated analogues 2-(2-aminoethoxy)ethanol (**2c**) and 2-((2-aminoethyl)amino)ethanol (**2d**) (Scheme 1a). The choice of primary amines was based on (i) the presence of a H-bond-donating group and (ii) different numbers of CH_2 groups attached to NH_2. All of these features can affect the formation of H-bonds and properties of the resulting compounds. It is known[24] that in the case of heterocyclic quinones **1a,b** nucleophilic substitution (carried out in an aprotic solvent) proceeds selectively and provides only the C(6) substituted product.

Compounds **3a−g** and **4a,b** possess H-bond-acceptor functionality (carbonyl groups) at one part and H-donor functionality (NH) at the opposite part of the molecule. In the case of compounds **3b−e** and **4b**, functional groups of the side chain can provide additional sites for the formation of H-bonds.

It is known[25] that hydrolysis of 6-*N*,*N*-diethylaminopyrido-[1,2-*a*]benzimidazole-8,9-dione led to the formation of the 1,4-quinone core. Interestingly, compound **5** (with an *o*-quinone core) was obtained during recrystallization of compound **3g** from ethanol (Scheme 2).

Scheme 2. Formation of Compound 5

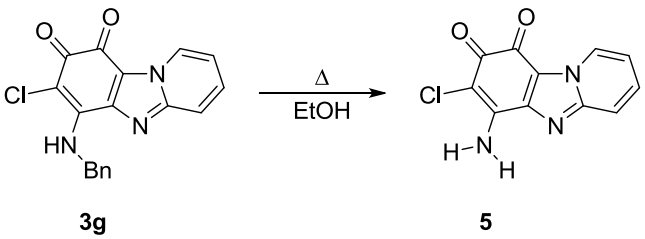

Additionally, signals of compound **5** and benzaldehyde were detected in a DMSO-d_6 solution of **3g** after 2 weeks by analysis of the ^{1}H NMR spectrum (Figure S36). The existence of the amino group was proved by ^{1}H NMR, two-dimensional (2D) ^{1}H−^{1}H nuclear Overhauser effect spectroscopy (NOESY), and 2D ^{1}H−^{1}H exchange spectroscopy (EXSY) NMR and Fourier-transform infrared (FTIR) spectra. It is worth mentioning that protons of the amino group were observed as two broad signals at 8.16 and 8.65 ppm (^{1}H NMR spectra in DMSO-d_6 solution, Figure S31), but addition of molecular sieves led to the coalescence of signals to one broad one that appeared at 8.41 ppm (Figure S35).

Single-Crystal X-ray Studies. The most demonstrative evidence of a H-bond existing in a crystal structure is the detection of close contacts via X-ray analysis. Diffraction data were collected at low temperatures on a Rigaku, XtaLAB Synergy, Dualflex, HyPix (Hybrid Pixel Array Detector) diffractometer using monochromated Cu−Kα radiation (λ = 1.54184 Å). An empirical absorption correction was performed using spherical harmonics, implemented in the SCALE3 ABSPACK scaling algorithm. The crystal structures were solved by direct methods using intrinsic phasing and refined by full-matrix least squares. All nonhydrogen atoms were refined in anisotropical approximation; hydrogen atoms involved in H-bonds were refined isotropically, and other H atoms were refined by the riding model. All calculations were performed with the help of Olex2 software.[26] Single-crystal X-ray crystallography data of compounds **3c−g** and **4a,b** can be found in the Supporting Information (Table S2, Figures S37−S51). For further details, see the crystallographic data for the compounds deposited at the Cambridge Crystallographic Data Centre (see Accession Codes in Supporting Information).

To avoid the formation of H-bonding between the *o*-quinone derivative and a protic solvent, aprotic solvent or solvents mixture (*n*-hexane, toluene, DCM, or acetonitrile) was used for the crystallization step. Only crystals of compound **3e** were obtained from methanol due to the poor solubility in aprotic solvents. Hirshfeld surfaces (for compounds **3c−d,g** and **4a,b**) and energy framework calculations[27] (for compounds **3c,g** and **4a,b**) were obtained (except for compounds **3e** and **3f** due to disorder of the crystal structure) in a whole-of molecule approach to explore intermolecular interactions in the crystal packing using the B3LYP/6-31G(d,p) energy model

https://doi.org/10.1021/acsomega.3c07005
ACS Omega 2023, 8, 40960−40971

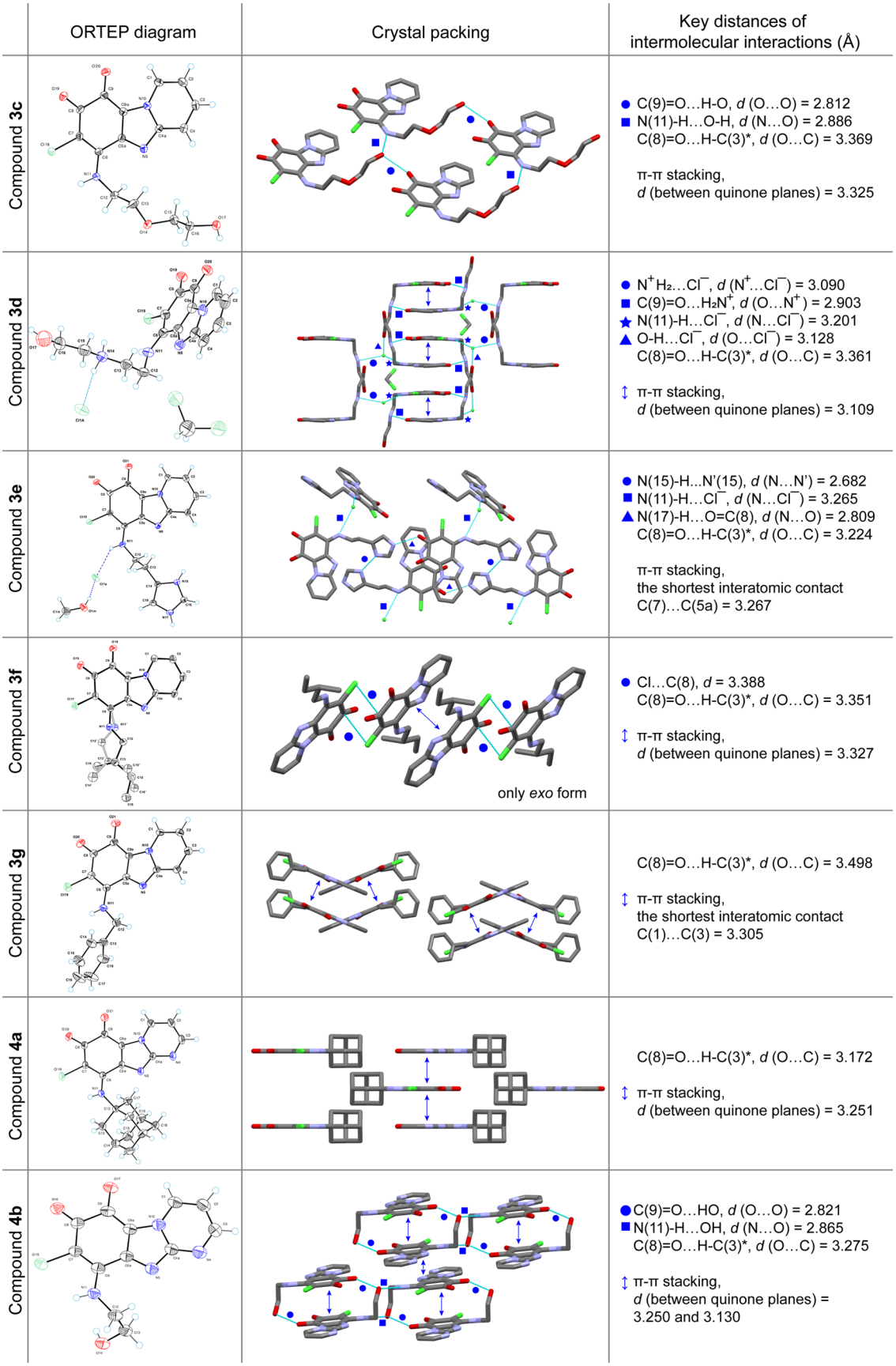

Figure 1. Oak ridge thermal ellipsoid plot (ORTEP) diagrams of the asymmetric unit for compounds **3c**−**g** and **4b** and the molecule of compound **4a** showing thermal ellipsoids at the 50% probability level. For the sake of clarity, all hydrogen atoms were omitted in the ORTEP diagram of compound **3f** and methanol molecules were omitted in the crystal packing of compound **3e**. Crystal packing with H-bonds and $\pi-\pi$ stacking marked with graphical symbols; key distances are listed, respectively. * This interaction is not shown in crystal packing.

https://doi.org/10.1021/acsomega.3c07005
ACS Omega 2023, 8, 40960−40971

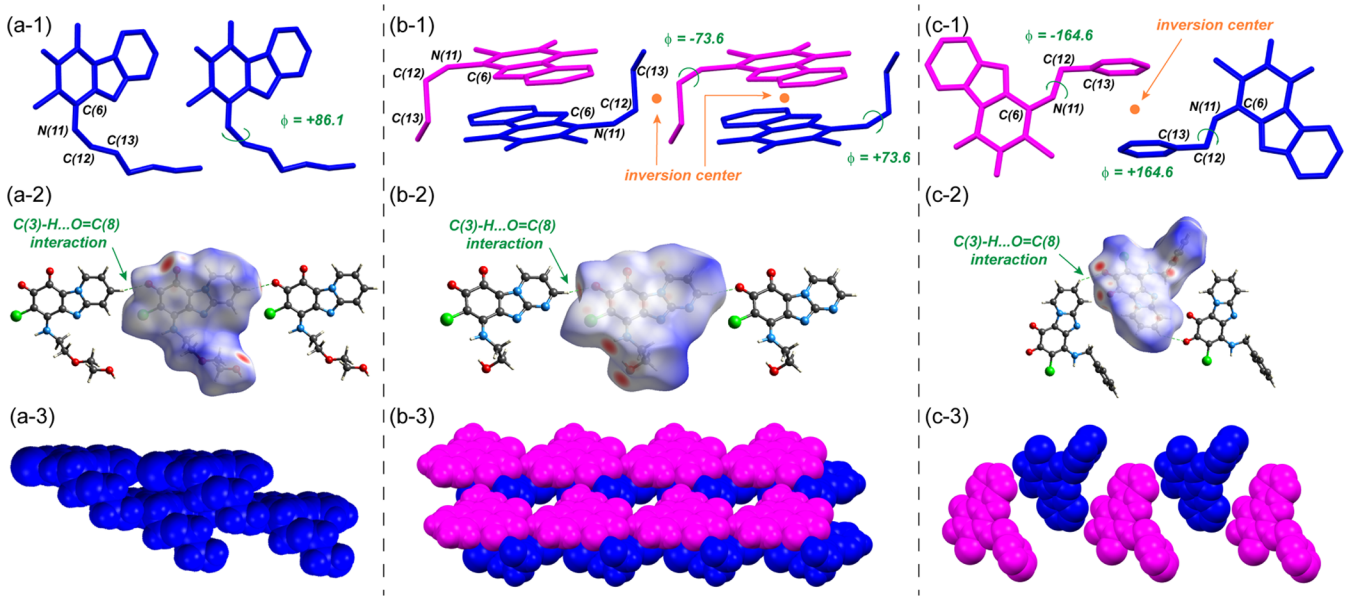

Figure 2. Crystal structures of (a) compound **3c**, (b) compound **4b**, and (c) compound **3g** were chosen as representatives of the (1) torsion angles of (+)-conformer (colored in blue) and (−)-conformer (colored in magenta). (2) Top view of Hirshfeld surfaces and 1D molecular chains with C(8)═O···H−C(3) contacts. (3) 1D hydrogen bonding motif: the (+)-conformer chain is shown in blue and the (−)-conformer chain is shown in magenta.

implemented in the CrystalExplorer21.5 program (Figures S52−S60).[28]

In the crystal structure of compounds **3c−g** and **4a,b**, a complicated balance between the various intermolecular forces was observed: in general, molecules of heterocyclic quinone derivatives are associated through strong to moderate[29] C(8)═O···H−C(3) H-bonds resulting in the formation of one-dimensional (1D) molecular chains. Heterocyclic quinone planes are held together by the $\pi-\pi$ stacking interactions that lead to the formation of layered motifs (2D structure). Functional groups of the amino substituent at the C(6) position determine different forms of intermolecular H-bonding of the side chains that resulted in three-dimensional (3D) H-bonded assemblies (Figures 1 and 2).

Crystal Structures. *Compound 3c.* Analysis of X-ray data showed that an achiral and conformationally flexible compound **3c** spontaneously crystallized into a noncentrosymmetric chiral crystal with the space group *P*1[30] with the Flack parameter close to zero. It is known[31] that the generation of chirality in the crystallization of achiral compounds is rare. Screening of 10 single crystals showed that the chirality of four of them corresponds to that of the crystal structure. For six single crystals, the crystal structure should be inverted. Thus, this substance represents a racemic conglomerate.

In the crystal packing of compound **3c**, a typical head-to-head columnar stacking was observed, which is essential for chiral crystallization.[31] H-bond networks were formed by the intermolecular interaction of OH···O═C(9) as well as NH···OH.

The architecture of crystal packing depends on the structure of the amino alcohol (e.g., distance from the OH group to the core), and changes such as replacement of the oxygen atom in the compound **3c** by the NH group (compound **3d**) lead to significant changes in intermolecular interactions.

Compound 3d. Compound **3d** was isolated as a salt with protonation occurring at the N(14) position due to the more pronounced basicity of this nitrogen compared to the other nitrogen atoms in the molecule. A complex 3D H-bond network was formed by C(9)═O···NH_2^+ interactions as well as intermolecular contacts between the chloride ion and proton-donor groups of three separate molecules simultaneously (Figure 1, vide infra Figure 4a).

Compound 3e. The X-ray data showed that chloride anions associated with molecular cations by means of H-bonds of the N(11)H···Cl^- type and imidazole hydrogens are not involved in this bond. The imidazole cycle is in the fully staggered position to N(11) through the CH_2-CH_2 group. The protonated imidazole ring has two NH protons, both participating in the formation of strong intermolecular H-bonds. One of the imidazole hydrogens takes part in the H-bond with the nitrogen atom of another imidazole ring that are typical for imidazole derivatives.[32] In the crystal structure of compound **3e**, methanol molecules lie on the second-order rotation axes of symmetry. Since such axes do not refer to the own symmetry of methanol molecules, the molecules can be only disordered. Thus, in compound **3e** occurred a so-called disorder by symmetry. Methanol molecules with chloride anions form strong enough hydrogen bonds of the OH···Cl type with the length of 3.113 Å (H(1m)···Cl(1a) = 2.19 Å, and O(1m)−H(1m)···Cl(1a) = 168°). Since molecules of CH_3OH lie on the 2-fold symmetry axis, the occupancy *g*-factors of all atoms of the molecules are equal to 0.5, i.e., the substance **3e** is a methanol semisolvate. It should be noted that the occupancy *g*-factor for the H(15) atom is 0.5 (as well as for the chloride anion, which lies on the 2-fold rotation axis of symmetry). Thus, compound **3e** represents a basic salt (Figure S42).

Compound 3f. Compound **3f** contains the aminoalkyl substituent at the C(6) position with the diastereotopic CH_2 group attached to N(11)H. The crystal structure of compound **3f** is achiral, and both configurations (*R* and *S*) of the C(13) atom are present since the racemic reagent **2f** was used. Interestingly, two molecular forms are found in crystals: *exo* and *endo* (vide infra, Figure 5a). The *endo* form is stabilized by an intramolecular H-bond of the NH···N type with the

https://doi.org/10.1021/acsomega.3c07005
ACS Omega 2023, 8, 40960−40971

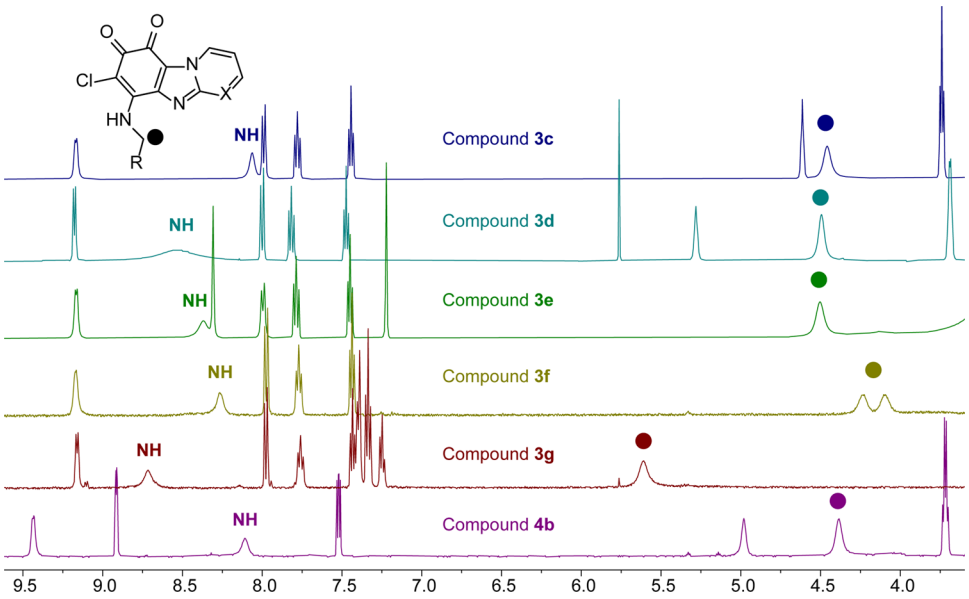

Figure 3. ^{1}H NMR (500 MHz, DMSO-d_6) spectra of compounds **3c–g** and **4b**; signals of αCH_2 protons are marked with circles.

following parameters: D···A *d* N(11′)···N(5) = 2.640 Å, N(11′)–H(11′)···N(5) = 114°. Because the *exo* and *endo* molecules or their mirror-image forms exist in the same crystallographic position, the crystal structure may be described with the help of the occupancy *g*-factors of the corresponding atoms. The main form (*exo* form) occupies 80%, while the *endo* form occupies 20%. The occupancy *g*-factors of atoms in the crystal structure (g = 0.8 and 0.2) were specified and fixed since at such values the thermal displacement parameters of the disordered atoms are close and have realistic values. At other values of *g*-factors, the thermal parameters become physically less realistic.

In the *exo* form, the methyl group (atom C(14)) is in the *gauche* position to nitrogen N(11), while the ethyl group (atoms C(15) and C(16)) is in the fully staggered position. In contrast, for the *endo* form, the methyl group (atom (C14′)) is in the fully staggered position to the amine nitrogen N(11′), but the ethyl group (atoms C(15′) and C(16′)) is in the *gauche* position. Despite the presence of the intramolecular H-bond, the *endo* form is a minor form in the crystals, which can be explained by an elongated C(6)–N(11′) bond in order to form an intramolecular H-bond (Table S3). Additionally, no strong intermolecular interactions were detected with the exception of the contact Cl···C(8), which can be interpreted as an π-hole interaction of medium strength.

*Compound **3g**.* In the solid state of compound **3g**, head-to-tail columnar stacking is found. Each of the C–H hydrogens of the methylene group has intermolecular H-bonds with carbonyl groups of the quinone fragment (C–H···O=C′(8) and C–H···O=C″(9)). A complicated balance between repulsion interactions of phenyl rings and heterocyclic quinone planes stacked through π–π stacking was observed (Figure S47). It is worth mentioning that in crystals of compound **3g**, a quite strong anisotropy of the imaginary part of the refraction index is observed. This leads to the fact that these crystals look red from one angle and greenish from another.

*Compound **4a**.* The main intermolecular interaction in the case of compound **4a** is the H-bond between C(3)-H···O= C(8) and stabilizing interlayer interactions between bulky adamantyl substituents.

*Compound **4b**.* In the case of compound **4b**, two modes of dimeric interactions were found in the crystal packing: H-bonds between the OH group of the substituent and carbonyl groups C(9)=O of *o*-quinone (centrosymmetric $R_2^2(20)$ dimer[33]) as well as H-bonds between aminoethanol side chains (centrosymmetric $R_2^2(8)$ dimer[33]). As a result, head-to-tail columnar stacking was accompanied by π–π stacking.

Crystal packing analysis revealed similarities and differences between intermolecular interactions in the crystal structures. In general, X-ray data showed that nitrogen (N(11)) at the C(6) position of all studied compounds has a planar configuration as the sum of angles (C(6)–N(11)–H, H–N(11)–C(12), and C(12)–N(11)–C(6)) is close to 360° (Table S3). This observation can lead to the conclusion that partially charged merocyanine exists in the O=C(8)–C(7)–C(6)–N(11)H fragment (Scheme 1b) and formation of conformers in the solid state can be explained by the restricted rotation along the C(6)–N(11) axis. The Mayer bond order of the C(6)–N(11) bond was calculated using *Multiwfn*[34] software from single-crystal X-ray analysis data of compounds **3c–g** and **4b**. Calculations proved the partial double-bond character of the C(6)–N(11) bond (Table S3). It is known that derivatives of **1a** tend to form compounds that can be characterized as coupled polymethines.[23] The partially charged merocyanine fragment can facilitate the formation of the resonance-assisted hydrogen bond.[35]

Analysis of X-ray data showed that the achiral compound **3c** crystallized into a noncentrosymmetric chiral crystal that contains only (+) synclinal conformers (Figure 2a-1). Crystallization of derivatives **3d–g** and **4b** resulted in the formation of centrosymmetric and, hence, achiral crystals. From the crystallography point of view, such structures can be interpreted as a single rotamer (one of a set of conformers arising from the restricted rotation about a single bond[36]) accompanied by its inverse equivalent. Because of torsional differences at C(6)–N(11)–C(12)-C(13) fragment, molecules of compounds **3d** and **4b** in centrosymmetric crystals acquire both (+) and (−) synclinal (30–90°), molecules of compound **3e**- (+) and (−) anticlinal (90–150°), and molecules of compounds **3f,g**- (+) and (−) antiperiplanar

https://doi.org/10.1021/acsomega.3c07005
ACS Omega 2023, 8, 40960–40971

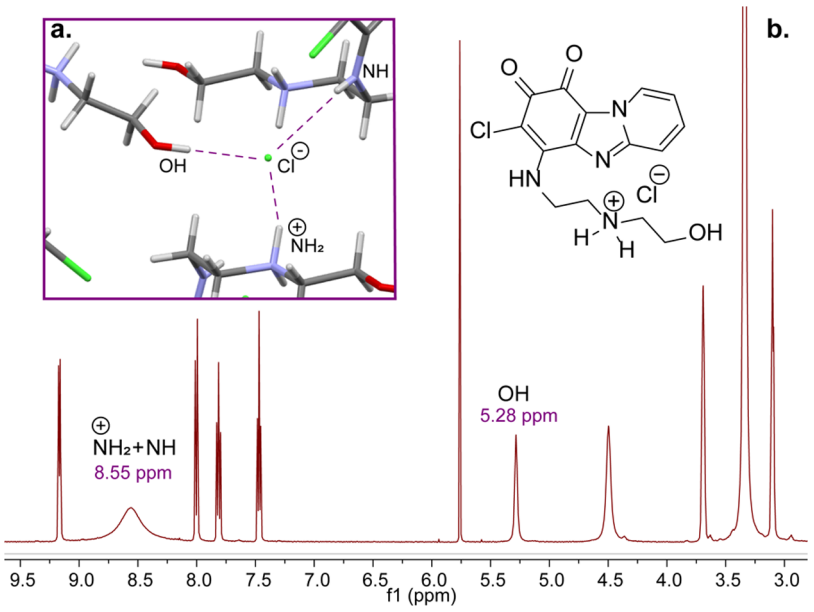

Figure 4. (a) Fragment of the H-bond network in the crystal packing of compound **3d** and (b) a fragment of the ^{1}H-spectrum of the compound **3d**.

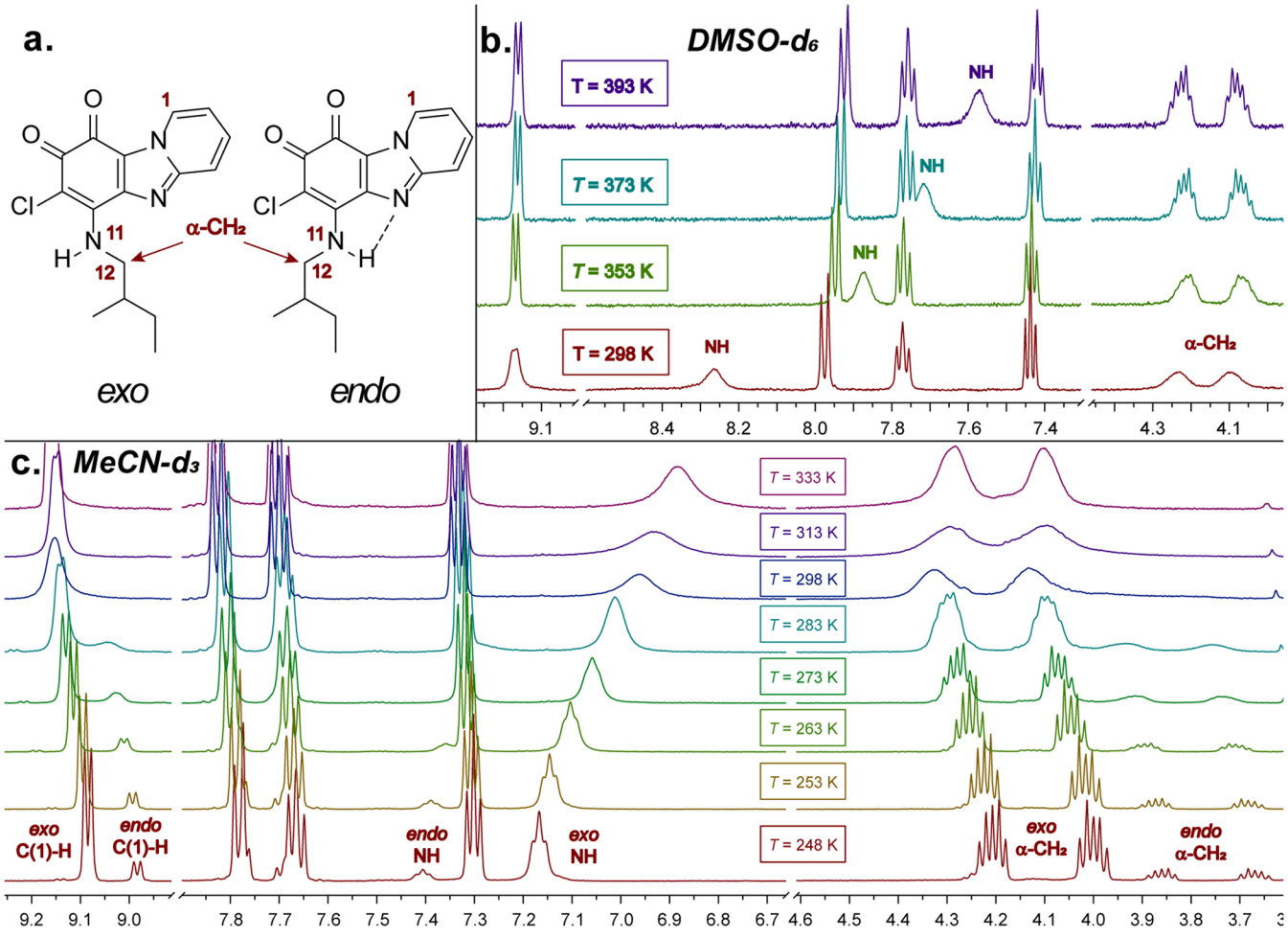

Figure 5. (a) Structures of *exo* and *endo* forms of compound **3f**. (b) Fragments of the VT ^{1}H NMR spectrum (500 MHz, DMSO-d_6) of compound **3f** in the temperature range of 298−393 K and (c) fragments of the VT ^{1}H NMR spectrum (500 MHz, MeCN-d_3) of compound **3f** in the temperature range of 248−333 K.

(150−180°) conformations (Figure 2a and Table S3). It was observed that antiperiplanar orientations were found in the crystal structure of compounds **3f** and **3g**, which bear a nonpolar substituent. Figure 2 shows a pair of conformers

https://doi.org/10.1021/acsomega.3c07005
ACS Omega 2023, 8, 40960−40971

connected by the inversion centers: blue-colored (+)-conformation and magenta-colored (−)-conformation. No conformers were detected in the case of compound **4a** due to the symmetrical structure of the introduced substituent and the absence of $-CH_2-$fragment necessary for the formation of a flexible moiety.

Molecules in the crystal structures of heterocyclic quinone derivatives (compounds **3c−g** and **4a,b**) are associated through strong to moderate[29] C(8)=O···H−C(3) H-bonds that lead to the formation of 1D molecular chains (Figures 1 and 2). Along this H-bond, 1D chains can be classified according to Kikkawa et al.[17] into two patterns: a straight pattern ([(+) or (−)] single conformer chains formed by H-bonds) observed in the case of compounds **3c−d,f** and **4b** (Figure 2a-3,b-3) and a zigzag pattern (chains that are formed through H-bonds and consisting of (+)- and (−)-conformers alternately associated with glide) in the case of compounds **3e** and **3g** (Figure 2c-3).

A common feature for all compounds is the $\pi-\pi$-stacking interaction that stabilizes head-to-head (compound **3c**) or head-to-tail (compounds **3d−g** and **4a,b**) columns. Distances between quinone planes lie in a range between 3.109 and 3.327 Å and are shorter than the sum of the van der Waals (vdW) radii (C 3.40 Å[37]). According to energy frameworks analysis, molecules are stacked in columns with dispersion dominated stacking. However, crystal structures of compound **3c** (Figure S53) and compound **4b** (Figure S57) represent balanced energy frameworks between electrostatic and dispersion contributions. Electrostatic energy is the largest for interaction between polar functional groups of flexible side chains; however, dispersion is the largest for the stacking motif between heterocyclic quinone planes.

NMR Spectroscopy. Analysis of ^{1}H NMR spectra (DMSO-d_6) (**3b−g** and **4b**) showed two remarkable features corresponding to the $-NH-\alpha CH_2-$ (i.e., $-N(11)-H-C(12)H_2-$) fragment: protons of αCH_2 appeared as broad-downfielded signals and NH proton signals were observed in the 7.99−8.72 ppm range (Figure 3).

Additionally, in the case of the hydrochloride salt **3d** NH and OH group signals were shifted downfield. It can be supposed that the trifurcated bond between the Cl^- anion, OH, and both NH/NH_2^+ groups (proved by single-crystal X-ray analysis in the solid state) exists in solution as well (Figure 4b).

To investigate the character of $-NH-\alpha CH_2-$ group signals, ^{1}H NMR spectra were recorded at 298 K in several solvents of different polarities and abilities to form H-bonds with the substrate. Compounds **3f** and **3g** were chosen due to their better solubility in less polar solvents such as MeCN-d_3 and $CDCl_3$. MeCN and $CHCl_3$ are solvents with a lower polarity and H-bond basicity[38] than DMSO, and chemical shifts of NH and αCH_2 protons can be sensitive to the solvent. Additionally, the existence of both forms (*endo* and *exo*) in solution (detected in the solid state in the case of compound **3f**, vide supra) was under consideration. To specify the diastereotopic protons of the αCH_2 group of compound **3f**, ^{1}H NMR resonance signals were assigned using 2D ^{1}H−^{1}H COSY and ^{1}H−^{13}C HSQC NMR spectra (Figures S17 and S18).

In DMSO-d_6 and MeCN-d_3 solutions at room temperature (298 K), signals of the *endo* form of compound **3f** were not detected. However, in a $CDCl_3$ solution, signals of both forms (*exo* and *endo*, Figure 5a) of compound **3f** were observed (Table 1 and Figure S15) with an *exo*/*endo* ratio of 70:30, which is close to the ratio observed in the crystal structure.

Table 1. Chemical Shifts (δ) of NH and αCH_2 Protons in the ^{1}H NMR Spectra (298 K) of Compounds 3f,g in Different Solvents

			chemical shifts (δ), ppm	
cmpd.	solvent	hydrogen-bond basicity of solvents (β_1)[38]	N*H*	HN-αC*H*$_2$
3f	DMSO-d_6	0.71	8.26	4.10, 4.23
	MeCN-d_3	0.37	6.96	4.33, 4.13
	$CDCl_3$	0	6.24^{exo}	4.09, 4.28^{exo}
			6.79^{endo}	3.74, 3.92^{endo}
3g	DMSO-d_6	0.71	8.72	5.69
	MeCN-d_3	0.37	~7.30	5.63
	$CDCl_3$	0	6.34	5.50

Interestingly, compound **3g** showed no separate signals of the *endo* form in the ^{1}H NMR spectra at 298 K in all three solvents used.

Solvent-dependent chemical shift of the NH signal is another notable feature. The formation of the solute−solvent complexes[39] between the NH proton and the solvent could explain a downfield shift of the NH signals in DMSO-d_6 relative to those in MeCN-d_3 and $CDCl_3$ for compounds **3f** and **3g**. Chemical shifts of the NH proton correlated well with the β_1 value (hydrogen-bond basicity)[38] of these solvents (Figures S16 and S28). Stabilization of the *exo* form by intermolecular interactions and formation of solute−solvent complexes in DMSO can compete with stabilization by an intramolecular H-bond that is well pronounced in less basic solvents.

The most remarkable feature of the ^{1}H NMR spectra of compounds **3b−g** and **4b** is a broad-downfielded signal of the αCH_2 protons in the DMSO-d_6 solution (Figure 3) as well as in MeCN-d_3 and $CDCl_3$ for compounds **3f** and **3g**. As the ^{1}H NMR spectra of all compounds containing the $NH-\alpha CH_2$ fragment have a broad signal of the αCH_2 protons, we supposed that compounds with no αCH_2 group can have a different behavior in solution. With this idea in mind, compounds **3a** and **4a** were synthesized. As expected, their ^{1}H NMR spectra can be easily interpreted and have no evidence of signal broadening (Figures S1 and S2) as well as no conformers detected in the crystal structure (vide supra).

Compounds **3b−e** and **4b** have the $-NH-\alpha CH_2-\underline{CH_2}$ fragment and signals of the $\underline{CH_2}$ group had clear splitting, suggesting that the broadening of the αCH_2 signal is not affected by the rest of the side chain. Several factors may explain the character of the αCH_2 signal, e.g., delocalization of electrons between N(11)H and C(8)=O groups (formation of the merocyanine fragment), which leads to a partially charged nitrogen.

In order to test the hindered rotation of the flexible side chain around the N(11)−C(12) bond in solution, quantum chemical calculations were utilized.[40] Geometry from X-ray data was used as initial structures for calculations of theoretical rotation barriers; conformation geometries were obtained by manually scanning along the torsion angle around the bond in question without relaxation of the remaining structure of the molecule. These structures were generated with Open Babel software.[41] For the (single-point) energy calculations, we used Gaussian 16, rev. C.01 computational software,[42] with a meta-hybrid functional MN15[43] and a double-hybrid functional DSD-PBEP86-D3(BJ),[44] which are reported in the literature to

https://doi.org/10.1021/acsomega.3c07005
ACS Omega 2023, 8, 40960−40971

be particularly suitable for computing both energy barriers and noncovalent interactions.[45,46] The results of these calculations (Figure S61) showed that the rotational barrier height ($\Delta G^{\ddagger}$) is around 2−4 kcal/mol for both compounds **3c** and **4b**, while a higher $\Delta G^{\ddagger}$ is observed for the compound **3d** (7 kcal/mol), as expected for cations. As the result of quantum chemical calculations, no evidence for high rotational barriers at the N(11)−C(12) bond of compounds **3c−d** and **4b** was provided; hence, dynamic rotational processes were excluded from consideration.

The cause of signal broadening could be nonequivalence of the αCH_2 protons because of the outcome of the unsymmetrical structure[47] or existence of *exo* and *endo* forms at room temperature, despite the fact that only the *exo* form crystallized in all cases with the exception of compound **3f**.

Typically, intramolecularly H-bonded structures are more stable; still, X-ray data showed that in cases of compounds **3c−g** and **4b** the *exo* form is major in the solid state. However, the existence of trace amounts of the *endo* form cannot be excluded and can explain the unusually strong widening of the αCH_2 resonance signal at room temperature. It is known[48] that intermolecular/intramolecular H-bonds are affected by elevated/low temperatures; thus, variable-temperature (VT) ^{1}H NMR experiments were carried out.

The impossibility of cooling the DMSO solution prevents full variable-temperature study for the compound **3c**; therefore, it was studied only at elevated temperatures (Figure S7). First, ^{1}H NMR resonance signals were assigned using a 2D ^{1}H−^{1}H-COSY spectrum (Figure S6). At 353 K the broad signal of the αCH_2 signal splits into a broad doublet. However, the NH proton is shifted upfield and the OH signal (initially appeared at 4.61 ppm) overlaps with the signal of water. The ^{1}H NMR spectrum of the cooled solution was identical to the first one acquired at room temperature except for the signal of the OH proton. Thus, protons of αCH_2, NH, and OH groups participate in the formation of intermolecular H-bonds in solution that were destroyed upon heating and restored back to room temperature.

We were able to follow the behavior of compounds **3f−g** (Figures 5, S21, and S29) with VT ^{1}H NMR experiments due to their sufficient solubility in MeCN-d_3 at temperatures lower than room temperature. ^{1}H NMR spectra (MeCN-d_3, 298 K) of both compounds **3f,g** (Figures 5c, S14, and S26) exhibited a set of broad signals corresponding to the signal of the NH group, αCH_2 protons as well as a signal of the proton at the C(1) position of the heterocyclic core.

The ^{1}H NMR spectrum of **3f** recorded in the MeCN-d_3 solution at 248 K showed narrowing and splitting of all broad signals (Figure 5c). An additional set of signals of low intensity (corresponding to the *endo* form) appeared, approving the existence of two forms (similar to the ^{1}H NMR spectrum in the $CDCl_3$ solution at room temperature). A low-intensity signal of the NH group appeared at 7.41 ppm ($\Delta\delta$ = 0.24 ppm with respect to the *exo* form) that apparently belongs to the intramolecularly H-bonded *endo* form. The ratio of the observed *exo*/*endo* forms at 248 K in the MeCN-d_3 solution was 85:15, which is in good agreement with the *exo*/*endo* ratio in the solid state. In general, the intermolecular H-bond is weaker[49] and, in turn, NH signals involved in such a type of H-bonding are more temperature-dependent than NH signals of the intramolecularly bonded group. Correlation between the NH proton (*exo* form) chemical shift and temperature is linear for solutions in DMSO-d_6 (298−393 K, R^2 = 0.99) and in MeCN-d_3 (248−333 K, R^2 = 0.97) (Figures S20 and S22). Diastereotopic protons of the *endo* form (αCH_2) showed clearly identifiable signals at 3.67 and 3.86 ppm and the signal of the C(1)-H proton appeared at 8.98 ppm with similar multiplicities as αCH_2 and C(1)-H of the *exo* form: as a result, C(1)-H and αCH_2 signals of the *endo* form shifted upfield (shielded), but the NH signal is downfield shifted (deshielded) relative to the signals of the *exo* form.

A single form of the compound **3f** was observed in the ^{1}H NMR spectrum upon heating in a DMSO-d_6 solution at 393 K. The multiplicity of each signal (αCH_2 group protons and C(1) proton) is similar to the multiplicity of the same signals in ^{1}H NMR spectra recorded at cooling for MeCN-d_3 solutions. It can be supposed that only the monomer *exo* form was found upon heating in DMSO-d_6 as H-bonds are weakened at elevated temperatures (Figure 5b). Cooling the solution of compound **3f** in DMSO-d_6 to room temperature restored the original spectrum acquired initially.

It should be mentioned that chemical shifts and multiplicity of signals of heterocyclic core protons (with the exception of C(1)-H) as well as the side-chain protons (with the exception of αCH_2 group protons) remained essentially unchanged during the cooling/heating processes.

The *endo* form of compound **3g** was also detected upon cooling in a MeCN-d_3 solution (Figure S30). At 253 K, αCH_2 protons of the *endo* form exhibited a doublet (J = 7.2 Hz) at 5.17 ppm and at the same time a doublet (J = 7.1 Hz) of the *exo* form appeared at 5.61 ppm. The ratio of *exo*/*endo* forms of compound **3g** was similar to the ratio of *exo*/*endo* forms for compound **3f** at low temperatures.

Temperature - gradients ($\Delta\delta_{HN}/\Delta T$)[48,49] were calculated for compounds where temperature dependence of the NH proton chemical shift was observed (Table S1). These results confirm our previous findings about stabilization of different solvate−solvent interactions by the solvent and do not exclude the influence of the rest of the side chain on the strength of H-bonds.

CONCLUSIONS

In summary, we synthesized pyrido- and pyrimido-[1,2-*a*]benzimidazole-8,9-dione derivatives in the reaction with simple primary amines and amino alcohols, providing the formation of the C−N bond. In the solid state, the derived compounds exist as partially charged merocyanines that lead to the restricted rotation along the C(6)−N(11) axis.

Crystallization of the resulting compounds led to different crystal structures where the noncentrosymmetric chiral crystal (**3c**) and centrosymmetric achiral crystals (**3d−g, 4a,b**) were detected. In the unit cell of centrosymmetric crystals, one rotamer and its inversion symmetry equivalent (with the opposite sign of torsion angle in the side chain) were found. Formation of 3D bonded networks due to multiple hydrogen bonds as well as other intermolecular interactions such as $\pi-\pi$ stacking and π−hole interaction was observed.

In the crystal structure of compound **3f**, two sets of different forms were observed: (1) (+)- and (−)-conformations characteristic to all derivatives with the −NH−CH_2− fragment; and (2) two forms with different relative orientations of the N−H bond with respect to quinone core: major *exo* (without an intramolecular H-bond) and minor *endo* (stabilized by an intramolecular H-bond) forms. Crystals of compounds **3c−e**, **3g**, and **4b** contain only the *exo* form. In a solution, due to intermolecular interactions of quinone

https://doi.org/10.1021/acsomega.3c07005
ACS Omega 2023, 8, 40960−40971

derivatives **3b−g** and **4b** with a proton-accepting solvent, the *exo* form is dominating; however, a less basic solvent (in the case of compound **3f**) increases the concentration of the *endo* form.

The selected compounds (**3f−g**) were chosen for the explanation of the unusual broadening of signals in ^{1}H NMR spectra in a series of heterocyclic quinone derivatives with the −NH−CH_2− fragment in the side chain. A combination of X-ray analysis, ^{1}H NMR, and VT ^{1}H NMR data was used. The observed broadening of the signals can be interpreted by the presence of a minor *endo* form at room temperature, despite the fact that only the *exo* form crystallized in all cases with the exception of compound **3f**. Our results suggest that caution should be exercised when interpreting such spectra.

The formation of a chiral crystal can be expected in the case of unsymmetrical merocyanine with a flexible side chain (−NH−CH_2− fragment); however, this assumption requires a more detailed investigation on a greater number of pyrido- and pyrimido-[1,2-*a*]benzimidazole-8,9-diones derivatives as well as different crystallization conditions should be explored.

METHODS

Reagents. Reagents and solvents were purified by standard means or used without further purification.

Analytical Methods and Apparatus. Melting points were measured on a Kruess KSP 11 Melting Point Analyzer. ^{1}H NMR and ^{13}C NMR spectra were recorded on the Bruker Avance 300 spectrometer or on the Bruker Avance 500 spectrometer (Bruker BioSpin GmbH, Rheinstetten, Germany) in DMSO-d_6, MeCN-d_3, or $CDCl_3$ solutions. Chemical shifts (δ) were reported in parts per million and coupling constants (J) in Hz. The proton signals for residual nondeuterated solvents (δ 7.26 for $CDCl_3$, δ 2.50 for DMSO-d_6, δ 1.94 for MeCN-d_3) and carbon signals (δ 77.1 for $CDCl_3$, δ 39.5 for DMSO-d_6) were used as an internal standard- 50 for ^{1}H NMR and ^{13}C NMR spectra, respectively. Elemental CHN analysis was carried on a Euro Vector EA 3000 analyzer. IR spectra were recorded on a PerkinElmer Spectrum 100 FTIR spectrometer. The UV−vis absorption spectra were acquired with a PerkinElmer 35 UV/vis spectrometer using 1 cm length quartz cuvettes with a concentration of compound $c = 2.5 \times 10^{-5}$ M. Low-resolution mass spectra were acquired on a Waters EMD 1000MS mass detector (ESI+ mode, voltage 30 V) with an Xterra MS C18 5 μm 2.1 100 mm column and a gradient eluent mode using 0.1% HCOOH in deionized water and MeCN or MeOH.

General Procedures and Characterization of Products. 6,7-Dichloropyrido[1,2-*a*]benzimidazole-8,9-dione **1a** and 6,7-dichloropyrimido[1,2-*a*]benzimidazole-8,9-dione **1b** were prepared according to previously reported procedures.[24]

Compounds **3a−g**, **4a,b** are too insoluble to record a qualitative ^{13}C NMR spectrum.

*Synthesis of Compounds **3a** and **4a**.* 1-Adamantanamine hydrochloride (precursor of **2a**, 0.53 g, 2.82 mmol) was dissolved in MeOH (5 mL), and a solution of KOH (0.16 g, 2.82 mmol) in MeOH was added. The resulting solution was stirred and then was added to a solution of 6,7-dichloropyrido-[1,2-*a*]benzimidazole-8,9-dione (**1a**) or 6,7-dichloropyrimido-[1,2-*a*]benzimidazole-8,9-dione (**1b**) (0.25 g, 0.94 mmol) in dichloromethane (DCM) (250 mL). The reaction mixture was stirred at room temperature for 72 h, and then, the reaction mixture was washed with water twice. The organic layer was dried over anhydrous $CaCl_2$ and evaporated under vacuum to get a dark-colored crude product. The precipitate was recrystallized from the DCM/*n*-hexane mixture and dried in air.

*6-(Adamantan-1-ylamino)-7-chlorobenzo[4,5]imidazo-[1,2-a]pyridine-8,9-dione (**3a**).* **Yield:** 0.12 g (34%), dark crystals. **MP**: 290 °C. **MS:** $C_{21}H_{20}ClN_3O_2$ requires $[M + H]^+$ 382.12; found $[M + H^+]^+$ 382.3. **^{1}H NMR (300 MHz, $CDCl_3$):** δ 9.28 (d, J = 6.5 Hz, 1H, H-1), 7.83 (d, J = 9.0 Hz, 1H, H-4), 7.61 (m, 1H, H-3), 7.23 (t, J = 6.8 Hz, 1H, H-2), 6.56 (br.s, 1H, exchanges with D_2O, NH), 2.42 (s, 6H, $CH_2 \times 3$), 2.24 (s, 3H, CH × 3), 1.79 (m, 6H, $CH_2 \times 3$). **IR (KBr pellet, cm^{-1}):** 3348, 3100, 3035, 2989, 2910, 2846, 1655, 1626, 1572, 1499, 1449. **Anal. Calcd** for $C_{21}H_{20}ClN_3O_2$ + 0.5 H_2O: C, 64.53; H, 5.42; N, 10.75; found C, 64.45; H, 5.17; N, 10.72.

*9-(Adamantan-1-ylamino)-8-chlorobenzo[4,5]imidazo-[1,2-a]pyrimidine-6,7-dione (**4a**).* **Yield:** 0.22 g (64%), dark crystals. **MP**: >300 °C. **MS:** $C_{20}H_{19}ClN_4O_2$ requires $[M + H]^+$ 383.12; found $[M + H^+]^+$ 383.3. **^{1}H NMR (300 MHz, $CDCl_3$):** δ 9.50 (d, J = 5.2 Hz, 1H, H-1), 8.86 (dd, J = 3.4; 1.6 Hz, 1H, H-3), 7.32 (dd, J = 5.3; 0.7 Hz, 1H, H-2), 6.66 (br.s, 1H, exchange with D_2O, NH), 2.45 (s, 6H, $CH_2 \times 3$), 2.26 (s, 3H, CH × 3), 1.81 (dd, J = 25.7, 12.1 Hz, 6H, $CH_2 \times 3$). **IR (KBr pellet, cm^{-1}):** 3434, 3343, 3108, 3075, 3014, 2907, 2850, 1658, 1633, 1615, 1572, 1522, 1459, 1425. **Anal. Calcd** for $C_{20}H_{19}ClN_4O_2$: C, 62.74; H, 5.00; N, 14.63; found C, 62.86; H, 5.14; N, 14.57.

*Synthesis of Compounds **3b** and **4b**.* 6,7-Dichloropyrido-[1,2-*a*]benzimidazole-8,9-dione (**1a**) or 6,7-dichloropyrimido-[1,2-*a*]benzimidazole-8,9-dione (**1b**) (0.2 g, 0.75 mmol) was dissolved in DCM (250 mL). Then, aminoethanol (**2b**, 0.14 mL, 2.25 mmol) was added to the resulting solution. A precipitate was formed after stirring the reaction mixture for 3 h. The solution was filtered, and the dark solid was washed with EtOH and MeCN three times.

*7-Chloro-6-((2-hydroxyethyl)amino)benzo[4,5]imidazo-[1,2-a]pyridine-8,9-dione (**3b**).* **Yield:** 0.13 g (62%), dark crystals. **MP**: >300 °C. **MS:** $C_{13}H_{10}ClN_3O_3$ requires $[M + H]^+$ 292.04; found $[M + H^+]^+$ 292.2. **^{1}H NMR (300 MHz, DMSO-d_6):** δ 9.16 (d, J = 6.0 Hz, 1H, H-1), 7.99 (d, J = 9.0 Hz, 2H, H-4 and NH (exchange with D_2O)), 7.78 (t, J = 8.0 Hz, 1H, H-3), 7.44 (t, J = 6.8 Hz, 1H, H-2), 4.96 (br.s, 1H, exchange with D_2O, OH), 4.36 (s, 2H, CH_2), 3.74 (q, J = 5.3 Hz, 2H, CH_2). **IR (KBr pellet, cm^{-1}):** 3380, 3195, 3087, 3024, 2967, 2922, 2874, 1650, 1616, 1571. **Anal. Calcd** for $C_{13}H_{10}ClN_3O_3$: C, 53.53; H, 3.46; N, 14.41; found C, 53.12; H, 3.70; N, 14.28.

*8-Chloro-9-((2-hydroxyethyl)amino)benzo[4,5]imidazo-[1,2-a]pyrimidine-6,7-dione (**4b**).* **Yield:** 0.08 g (37%), dark crystals. **MP**: 228−230 °C. **MS:** $C_{13}H_{10}ClN_3O_3$ requires $[M + H]^+$ 292.0; found $[M + H^+]^+$ 292.2. **^{1}H NMR (300 MHz, DMSO-d_6):** δ 9.43 (d, J = 5.4 Hz, 1H, H-1), 8.91 (dd, J = 4.0; 1.6 Hz, 1H, H-3), 7.52 (dd, J = 6.5; 4.5 Hz, 1H, H-2), 5.00 (br.s, 1H, exchange with D_2O, OH), 4.37 (s, 2H, CH_2), 3.71 (m, 2H, CH_2). **IR (KBr pellet, cm^{-1}):** 3391, 3184, 1654, 1611, 1563, 1524, 1473, 1427. **Anal. Calcd** for $C_{13}H_{10}ClN_3O_3$+0.5H_2O C, 47.77; H, 3.34; N, 18.57; found C, 47.84; H, 3.66; N, 18.25.

*7-Chloro-6-((2-(2-hydroxyethoxy)ethyl)amino)benzo[4,5]-imidazo[1,2-a]pyridine-8,9-dione (**3c**).* To a solution of 6,7-dichloropyrido[1,2-*a*]benzimidazole-8,9-dione (**1a**, 0.2 g, 0.75 mmol) in DCM (300 mL), 2-(2-aminoetoxy)ethanol (**2c**, 0.19 mL, 1.88 mmol) was added. The solution was stirred for 4 h, and then, the reaction mixture was washed with water. The

https://doi.org/10.1021/acsomega.3c07005
ACS Omega 2023, 8, 40960−40971

organic layer was dried over anhydrous $CaCl_2$ and evaporated under vacuum to get a dark-colored crude product. The precipitate was recrystallized from MeCN and dried in air. **Yield:** 0.15 g (60%), dark crystals. **MP**: 218−220 °C. **^{1}H NMR (500 MHz, DMSO-d_6):** δ 9.17 (d, J = 5.6 Hz, 1H, H-1), 8.06 (br.s, 1H, exchange with D_2O, NH), 7.99 (d, J = 9.0 Hz, 1H, H-4), 7.78 (t, J = 8.0 Hz, 1H, H-3), 7.44 (t, J = 6.8 Hz, 1H, H-2), 4.61 (s, 1H, exchange with D_2O, OH), 4.46 (s, 2H, CH_2), 3.74 (t, J = 5.9 Hz, 2H, CH_2), 3.50 (s, 4H, CH_2). **IR (KBr pellet, cm^{-1}):** 3396, 3228, 3084, 2947, 2867, 1715, 1651, 1626, 1569, 1425. **Anal. Calcd** for $C_{15}H_{14}ClN_3O_4$: C, 53.66; H, 4.20; N, 12.52; found C, 53.80; H, 4.23; N, 12.61.

*2-((7-Chloro-8,9-dioxo-8,9-dihydrobenzo[4,5]imidazo-[1,2-a]pyridin-6-yl)amino)-N-(2-hydroxyethyl)-ethanaminium chloride (**3d**).* To a solution of 6,7-dichloropyrido[1,2-*a*]benzimidazole-8,9-dione (**1a**) (0.15 g, 0.56 mmol) in DCM, 2-(2-aminoethylamino)ethanol (**2d**, 0.14 mL, 1.40 mmol) was added. The solution was stirred for 4 h. A dark-colored precipitate was formed and filtered. The precipitate was washed with EtOH and MeCN three times and dried in air. **Yield:** 0.13 g (65%), dark crystals. **MP**: 229−232 °C. **^{1}H NMR (500 MHz, DMSO-d_6):** δ 9.17 (d, J = 6.6 Hz, 1H, H-1), 8.55 (br.s, 3H, exchange with D_2O, NH), 8.00 (d, J = 9.0 Hz, 1H, H-4), 7.81 (t, J = 8.0 Hz, 1H, H-3), 7.47 (t, J = 6.9 Hz, 1H, H-2), 5.28 (s, 1H, exchange with D_2O, OH), 4.43 (s, 2H, CH_2), 3.69 (s, 2H, CH_2), 3.36 (overlaps with H_2O signal, t, J = 5.8 Hz, 2H, CH_2), 3.10 (t, J = 5.1 Hz, 2H, CH_2). **IR (KBr pellet, cm^{-1}):** 3368, 3187, 3040, 2826, 1648, 1616, 1563, 1535, 1522, 1497, 1447. **Anal. Calcd** for $C_{15}H_{16}Cl_2N_4O_3$+0.5CH_2Cl_2: C, 45.79; H, 4.08; N, 13.35; found C, 45.41; H, 4.46; N, 13.76.

*6-((2-(1H-Imidazol-4-yl)ethyl)amino)-7-chlorobenzo[4,5]-imidazo[1,2-a]pyridine-8,9-dione (**3e**).* Histamine dihydrochloride (precursor of **2e**, 0.2 g, 1.12 mmol) was dissolved in MeOH (5 mL), and a solution of KOH (0.12 g, 2.24 mmol) in MeOH was added. The resulting solution was added to a solution of 6,7-dichloropyrido[1,2-*a*]benzimidazole-8,9-dione (**1a**, 0.15 g, 0.56 mmol) in DCM (250 mL). The reaction mixture was stirred at room temperature for 72 h. The organic layer was evaporated under vacuum until 20 mL to get a dark-colored crude product. The dark-colored precipitate was filtrated, recrystallized from MeOH, and dried in air. **Yield:** 0.12 g (63%), dark powder. **MP**: 225−227 °C. **MS:** $C_{16}H_{12}ClN_5O_2$ requires $[M + H]^+$ 342.1; found $[M + H^+]^+$ 342.3. **^{1}H NMR (500 MHz, DMSO-d_6):** δ 9.17 (d, J = 5.7 Hz, 1H, H-1), 8.37 (br.s, 1H, exchange with D_2O, NH), 8.31 (s, 1H, $CH_{imidazole}$), 8.00 (d, J = 8.8 Hz, 1H, H-4), 7.79 (t, J = 8.0 Hz, 1H, H-3), 7.45 (t, J = 6.9 Hz, 1H, H-2), 7.22 (s, 1H, $CH_{imidazole}$), 4.50 (s, 2H, CH_2), 3.05 (t, J = 6.7 Hz, 2H, CH_2). **IR (KBr pellet, cm^{-1}):** 3291, 3145, 2886, 2814, 163, 1660, 1609, 1547, 1514. **Anal. Calcd** for $C_{16}H_{12}ClN_5O$ + 0.5 Cl + 0.5 CH_3OH ($C_{33}H_{29}Cl_3N_{10}O_5$ known from X-ray analysis) C, 52.71; H, 3.89; N, 18.63; found C, 52.74; H, 4.04; N, 18.42.

*7-Chloro-6-((2-methylbutyl)amino)benzo[4,5]imidazo-[1,2-a]pyridine-8,9-dione (**3f**).* 6,7-Dichloropyrido[1,2-*a*]-benzimidazole-8,9-dione (**1a**) (0.2 g, 0.75 mmol) was dissolved in DCM (250 mL). Then, isopentylamine (**2f**, 0.16 mL, 1.88 mmol) was added to the resulting solution. The reaction mixture was stirred at room temperature for 2 h. Then, the reaction mixture in DCM was washed with water twice. The organic layer was dried over anhydrous $CaCl_2$ and evaporated under vacuum to get a dark-colored crude product. The precipitate was recrystallized from a toluene/*n*-hexane mixture and was dried in air. **Yield:** 0.11 g (65%), dark powder. **MP**: 174−176 °C. **MS:** $C_{16}H_{16}ClN_3O_2$ requires $[M + H]^+$ 318.1; found $[M + H^+]^+$ 318.4. **^{1}H NMR (500 MHz, DMSO-d_6):** δ 9.17 (d, J = 3.5 Hz, 1H, H-1), 8.27 (br.s, 1H, exchange with D_2O, NH), 7.97 (d, J = 9.0 Hz, 1H, H-4), 7.77 (t, J = 7.9 Hz, 1H, H-3), 7.44 (t, J = 6.9 Hz, 1H, H-2), 4.10 (s, 1H, CH_2 (diastereotopic)), 4.23 (s, 1H, CH_2 (diastereotopic)), 1.86 (dq, J = 12.9, 6.6 Hz, 1H, CH), 1.48 (dt, J = 12.8, 6.8 Hz, 1H, CH_2 (diastereotopic)), 1.20 (dd, J = 13.9, 7.3 Hz 1H, CH_2 (diastereotopic)), 0.92 (dd, J = 7.3, Hz, 6H, 2 × CH_3). **IR (KBr pellet, cm^{-1}):** 3468, 3371, 3082, 3022, 2962, 2875, 1655, 1626, 1571, 1494. **Anal. Calcd** for $C_{16}H_{16}ClN_3O_2$ C, 60.47; H, 5.08; N, 13.22; found C, 60.81; H, 5.22; N, 13.05.

*6-(Benzylamino)-7-chlorobenzo[4,5]imidazo[1,2-a]-pyridine-8,9-dione (**3g**).* 6,7-Dichloropyrido[1,2-*a*]-benzimidazole-8,9-dione (**1a**) (0.2 g, 0.75 mmol) was dissolved in DCM (250 mL). Then, benzylamine (**2g**, 0.14 mL, 2.25 mmol) was added to the resulting solution. The reaction mixture was stirred at room temperature for 24 h and then was washed with water twice. The organic layer was dried over anhydrous $CaCl_2$ and evaporated under vacuum to get a dark-colored crude product. The precipitate was recrystallized from the DCM/*n*-hexane mixture and was dried in air. **Yield:** 0.14 g (67%), dark powder. **MP**: 174−177 °C. **MS:** $C_{18}H_{12}ClN_3O_2$ requires $[M + H]^+$ 338.1; found $[M + H^+]^+$ 338.3. **^{1}H NMR (500 MHz, DMSO-d_6):** δ 9.16 (d, J = 6.4 Hz, 1H, H-1), 8.72 (br.s, 1H, exchange with D_2O, NH), 7.98 (d, J = 9.0 Hz, 1H, H-4), 7.76 (t, J = 8.1 Hz, 1H, H-3), 7.43 (t, J = 6.9 Hz, 1H, H-2), 7.40 (d, J = 7.4 Hz, 2H, $CH_{arom.}$), 7.34 (t, J = 7.6 Hz, 2H, $CH_{arom.}$), 7.25 (t, J = 7.2 Hz, 1H, $CH_{arom.}$), 5.61 (s, 1H, CH_2). **IR (KBr pellet, cm^{-1}):** 3438, 3359, 3105, 3040, 2885, 1665, 1623, 1569, 1497. **Anal. Calcd** for $C_{18}H_{12}ClN_3O_2$ C, 64.01; H, 3.58; N, 12.44; found C, 63.61; H, 3.74; N, 12.37.

*6-Amino-7-chlorobenzo[4,5]imidazo[1,2-a]pyridine-8,9-dione (**5**).* **Yield:** 0.04 g (51%), dark-red crystals. **MP**: >300 °C. **MS:** $C_{11}H_6ClN_3O_2$ requires $[M + H]^+$ 248.1; found $[M + H^+]^+$ 248.3. **^{1}H NMR (500 MHz, DMSO-d_6):** δ 9.10 (d, J = 6.7 Hz, 1H, H-1), 8.65 (br.s, 1H, exchange with D_2O, NH), 8.15 (br.s, 1H, exchange with D_2O, NH), 7.95 (d, J = 9.0 Hz, 1H, H-4), 7.78 (m, 1H, H-3), 7.43 (t, J = 6.9 Hz, 1H, H-2). **^{13}C NMR (125 MHz, DMSO-d_6):** 171.9, 168.6, 148.9, 148.5, 147.3, 132.1 (CH), 128.6 (CH), 119.2, 118.6 (CH), 118.3 (CH), 114.9. **IR (KBr pellet, cm^{-1}):** 3448, 3246, 3204, 1657, 1628, 1583, 1542, 1501, 1448. **Anal. Calcd** for $C_{11}H_6ClN_3O_2$ C, 53.80; H, 2.44; N, 16.97; found C, 53.87; H, 2.71; N, 16.65.

■ ASSOCIATED CONTENT

Data Availability Statement

The data underlying this study are available in the published article and its Supporting Information.

Supporting Information

The Supporting Information is available free of charge at https://pubs.acs.org/doi/10.1021/acsomega.3c07005.

Figures of ^{1}H NMR spectra (for compounds **3a**−**g**, **4a**,**b**, and **5**), 2D ^{1}H−^{1}H COSY NMR spectra (for compounds **3c**−**f**), ^{1}H−^{13}C HSQC NMR spectra (for compound **3f**) as well as full VT ^{1}H NMR spectra for compound **3c** (in DMSO-d_6 solution), compound **3f** (in DMSO-d_6 and MeCN-d_3 solutions), and compound **3g** (in MeCN-d_3 solution); single-crystal X-ray analysis data with ORTEP diagrams of the asymmetric unit for compounds **3c**−**g** and **4a**,**b**; and figures of Hirshfeld

https://doi.org/10.1021/acsomega.3c07005
ACS Omega 2023, 8, 40960−40971

surfaces and energy frameworks calculated with CrystalExplorer software (PDF)

AUTHOR INFORMATION

Corresponding Author

Nelli Batenko − *Riga Technical University, Faculty of Materials Science and Applied Chemistry, Riga LV-1048, Latvia*; Email: nelli.batenko@rtu.lv

Authors

Anastasija Gaile − *Riga Technical University, Faculty of Materials Science and Applied Chemistry, Riga LV-1048, Latvia*; orcid.org/0000-0001-7268-573X

Sergey Belyakov − *Latvian Institute of Organic Chemistry, Riga LV-1006, Latvia*

Vitālijs Rjabovs − *Riga Technical University, Faculty of Materials Science and Applied Chemistry, Riga LV-1048, Latvia*

Igors Mihailovs − *Riga Technical University, Faculty of Computer Science and Information Technology, Riga LV-1048, Latvia; University of Latvia, Institute of Solid State Physics, Riga LV-1063, Latvia*

Baiba Turovska − *Latvian Institute of Organic Chemistry, Riga LV-1006, Latvia*

Complete contact information is available at: https://pubs.acs.org/10.1021/acsomega.3c07005

Author Contributions

N.B.: Supervision, conceptualization, writing—original draft, review and editing. A.G.: Investigation, writing—original draft, review and editing, visualization, funding acquisition. S.B., V.R., and B.T.: Investigation. I.M.: Formal analysis. All authors approved the final version of the manuscript.

Notes

The authors declare no competing financial interest.

ACKNOWLEDGMENTS

This work was supported by the European Social Fund within Project No. 8.2.2.0/20/I/008 ≪Strengthening of PhD students and academic personnel of Riga Technical University and BA School of Business and Finance in the strategic fields of specialization≫ of the Specific Objective 8.2.2 ≪To Strengthen Academic Staff of Higher Education Institutions in Strategic Specialization Areas≫ of the Operational Programme ≪Growth and Employment≫. This research/publication was supported by Riga Technical University's Doctoral Grant program (DOK.LKI/21).

REFERENCES

(1) De Causmaecker, S.; Douglass, J. S.; Fantuzzi, A.; Nitschke, W.; Rutherford, A. W. Energetics of the Exchangeable Quinone, Q B, in Photosystem II. *Proc. Natl. Acad. Sci. U.S.A.* **2019**, *116* (39), 19458−19463.

(2) Anand, A.; Chen, K.; Yang, L.; Sastry, A. V.; Olson, C. A.; Poudel, S.; Seif, Y.; Hefner, Y.; Phaneuf, P. V.; Xu, S.; Szubin, R.; Feist, A. M.; Palsson, B. O. Adaptive Evolution Reveals a Tradeoff between Growth Rate and Oxidative Stress during Naphthoquinone-Based Aerobic Respiration. *Proc. Natl. Acad. Sci. U.S.A.* **2019**, *116* (50), 25287−25292.

(3) Ji, Q.; Zhang, L.; Jones, M. B.; Sun, F.; Deng, X.; Liang, H.; Cho, H.; Brugarolas, P.; Gao, Y. N.; Peterson, S. N.; Lan, L.; Bae, T.; He, C. Molecular Mechanism of Quinone Signaling Mediated through S-Quinonization of a YodB Family Repressor QsrR. *Proc. Natl. Acad. Sci. U.S.A.* **2013**, *110* (13), 5010−5015.

(4) Bolton, J. L.; Dunlap, T. Formation and Biological Targets of Quinones: Cytotoxic versus Cytoprotective Effects. *Chem. Res. Toxicol.* **2017**, *30* (1), 13−37.

(5) Salazar, C. A.; Flesch, K. N.; Haines, B. E.; Zhou, P. S.; Musaev, D. G.; Stahl, S. S. Tailored Quinones Support High-Turnover Pd Catalysts for Oxidative C−H Arylation with O 2. *Science* **2020**, *370* (6523), 1454−1460.

(6) Piera, J.; Bäckvall, J.-E. Catalytic Oxidation of Organic Substrates by Molecular Oxygen and Hydrogen Peroxide by Multistep Electron Transfer—A Biomimetic Approach. *Angew. Chem., Int. Ed.* **2008**, *47* (19), 3506−3523.

(7) Wang, F.; Sheng, H.; Li, W.; Gerken, J. B.; Jin, S.; Stahl, S. S. Stable Tetrasubstituted Quinone Redox Reservoir for Enhancing Decoupled Hydrogen and Oxygen Evolution. *ACS Energy Lett.* **2021**, 1533−1539.

(8) Son, E. J.; Kim, J. H.; Kim, K.; Park, C. B. Quinone and Its Derivatives for Energy Harvesting and Storage Materials. *J. Mater. Chem. A* **2016**, *4* (29), 11179−11202.

(9) Han, C.; Li, H.; Shi, R.; Zhang, T.; Tong, J.; Li, J.; Li, B. Organic Quinones towards Advanced Electrochemical Energy Storage: Recent Advances and Challenges. *J. Mater. Chem. A* **2019**, *7* (41), 23378−23415.

(10) Sieuw, L.; Jouhara, A.; Quarez, É.; Auger, C.; Gohy, J.-F.; Poizot, P.; Vlad, A. A H-Bond Stabilized Quinone Electrode Material for Li−Organic Batteries: The Strength of Weak Bonds. *Chem. Sci.* **2019**, *10* (2), 418−426.

(11) Tuttle, M. R.; Davis, S. T.; Zhang, S. Synergistic Effect of Hydrogen Bonding and $\pi-\pi$ Stacking Enables Long Cycle Life in Organic Electrode Materials. *ACS Energy Lett.* **2021**, *6* (2), 643−649.

(12) Lin, Z.; Shi, H.-Y.; Lin, L.; Yang, X.; Wu, W.; Sun, X. A High Capacity Small Molecule Quinone Cathode for Rechargeable Aqueous Zinc-Organic Batteries. *Nat. Commun.* **2021**, *12* (1), No. 4424.

(13) Tong, L.; Jing, Y.; Gordon, R. G.; Aziz, M. J. Symmetric All-Quinone Aqueous Battery. *ACS Appl. Energy Mater.* **2019**, *2* (6), 4016−4021.

(14) Wang, C. Weak Intermolecular Interactions for Strengthening Organic Batteries. *Energy Environ. Mater.* **2020**, *3* (4), 441−452.

(15) Zheng, S.; Shi, D.; Sun, T.; Zhang, L.; Zhang, W.; Li, Y.; Guo, Z.; Tao, Z.; Chen, J. Hydrogen Bond Networks Stabilized High-Capacity Organic Cathode for Lithium-Ion Batteries. *Angew. Chem., Int. Ed.* **2023**, *62* (9), No. e202217710, DOI: 10.1002/anie.202217710.

(16) Langis-Barsetti, S.; Maris, T.; Wuest, J. D. Triptycene 1,2-Quinones and Quinols: Permeable Crystalline Redox-Active Molecular Solids. *J. Org. Chem.* **2018**, *83* (24), 15426−15437.

(17) Kikkawa, S.; Masu, H.; Katagiri, K.; Okayasu, M.; Yamaguchi, K.; Danjo, H.; Kawahata, M.; Tominaga, M.; Sei, Y.; Hikawa, H.; Azumaya, I. Characteristic Hydrogen Bonding Observed in the Crystals of Aromatic Sulfonamides: 1D Chain Assembly of Molecules and Chiral Discrimination on Crystallization. *Cryst. Growth Des.* **2019**, *19* (5), 2936−2946.

(18) Corpinot, M. K.; Bučar, D.-K. A Practical Guide to the Design of Molecular Crystals. *Cryst. Growth Des.* **2019**, *19* (2), 1426−1453.

(19) Formen, J. S. S. K.; Wolf, C. Chiroptical Switching and Quantitative Chirality Sensing with (Pseudo)Halogenated Quinones. *Angew. Chem., Int. Ed.* **2021**, *60* (52), 27031−27038.

(20) Helmers, I.; Ghosh, G.; Albuquerque, R. Q.; Fernández, G. Pathway and Length Control of Supramolecular Polymers in Aqueous Media via a Hydrogen Bonding Lock. *Angew. Chem., Int. Ed.* **2021**, *60* (8), 4368−4376.

(21) Edwards, A. J.; Mackenzie, C. F.; Spackman, P. R.; Jayatilaka, D.; Spackman, M. A. Intermolecular Interactions in Molecular Crystals: What's in a Name? *Faraday Discuss.* **2017**, *203*, 93−112.

(22) Mutai, T.; Muramatsu, T.; Yoshikawa, I.; Houjou, H.; Ogura, M. Development of Imidazo[1,2-a]Pyridine Derivatives with an Intramolecular Hydrogen-Bonded Seven-Membered Ring Exhibiting

Bright ESIPT Luminescence in the Solid State. *Org. Lett.* **2019**, *21* (7), 2143−2146.
(23) Gaile, A.; Belyakov, S.; Turovska, B.; Batenko, N. Synthesis of Asymmetric Coupled Polymethines Based on a 7-Chloropyrido[1,2- a]Benzimidazole-8,9-Dione Core. *J. Org. Chem.* **2022**, *87* (5), 2345−2355.
(24) Batenko, N.; Belyakov, S.; Kiselovs, G.; Valters, R. Synthesis of 6,7-Dichloropyrido[1,2-a]Benzimidazole-8,9-Dione and Its Analogues and Their Reactions with Nucleophiles. *Tetrahedron Lett.* **2013**, *54* (35), 4697−4699.
(25) Batenko, N.; Kricka, A.; Belyakov, S.; Turovska, B.; Valters, R. A Novel Method for the Synthesis of Benzimidazole-Based 1,4-Quinone Derivatives. *Tetrahedron Lett.* **2016**, *57* (3), 292−295.
(26) Dolomanov, O. V.; Bourhis, L. J.; Gildea, R. J.; Howard, J. A. K.; Puschmann, H. OLEX2: A Complete Structure Solution, Refinement and Analysis Program. *J. Appl. Crystallogr.* **2009**, *42* (2), 339−341.
(27) Turner, M. J.; Thomas, S. P.; Shi, M. W.; Jayatilaka, D.; Spackman, M. A. Energy Frameworks: Insights into Interaction Anisotropy and the Mechanical Properties of Molecular Crystals. *Chem. Commun.* **2015**, *51* (18), 3735−3738.
(28) Spackman, P. R.; Turner, M. J.; McKinnon, J. J.; Wolff, S. K.; Grimwood, D. J.; Jayatilaka, D.; Spackman, M. A. CrystalExplorer : A Program for Hirshfeld Surface Analysis, Visualization and Quantitative Analysis of Molecular Crystals. *J. Appl. Crystallogr.* **2021**, *54* (3), 1006−1011.
(29) Giacovazzo, C.; Monaco, H.; Artioli, G.; Viterbo, D.; Ferraris, G.; Gilli, G.; Zanotti, G.; Catti, M. *Fundamentals of Crystallography*, 2nd ed.; Oxford University Press, 2002.
(30) Adawy, A. Functional Chirality: From Small Molecules to Supramolecular Assemblies. *Symmetry* **2022**, *14* (2), 292.
(31) Matsuura, T.; Koshima, H. Introduction to Chiral Crystallization of Achiral Organic Compounds: Spontaneous Generation of Chirality. *J. Photochem. Photobiol., C* **2005**, *6* (1), 7−24.
(32) Miao, Y.; Fu, R.; Zhou, H.-X.; Cross, T. A. Dynamic Short Hydrogen Bonds in Histidine Tetrad of Full-Length M2 Proton Channel Reveal Tetrameric Structural Heterogeneity and Functional Mechanism. *Structure* **2015**, *23* (12), 2300−2308.
(33) Etter, M. C.; MacDonald, J. C.; Bernstein, J. Graph-set Analysis of Hydrogen-bond Patterns in Organic Crystals. *Acta Crystallogr., Sect. B: Struct. Sci.* **1990**, *46* (2), 256−262.
(34) Lu, T.; Chen, F. Multiwfn: A Multifunctional Wavefunction Analyzer. *J. Comput. Chem.* **2012**, *33* (5), 580−592.
(35) Steiner, T. The Hydrogen Bond in the Solid State. *Angew. Chem., Int. Ed.* **2002**, *41*, 48−76.
(36) Eliel, L. E.; Wilen, H. S. *Stereochemistry of Organic Compounds*; John Wiley & Sons, Inc.: New York, 1994.
(37) Mantina, M.; Chamberlin, A. C.; Valero, R.; Cramer, C. J.; Truhlar, D. G. Consistent van Der Waals Radü for the Whole Main Group. *J. Phys. Chem. A* **2009**, *113* (19), 5806−5812.
(38) Laurence, C.; Legros, J.; Chantzis, A.; Planchat, A.; Jacquemin, D. A Database of Dispersion-Induction DI, Electrostatic ES, and Hydrogen Bonding A1and Δ1solvent Parameters and Some Applications to the Multiparameter Correlation Analysis of Solvent Effects. *J. Phys. Chem. B* **2015**, *119* (7), 3174−3184.
(39) Sigalov, M.; Shainyan, B.; Chipanina, N.; Ushakov, I.; Shulunova, A. Intra- and Intermolecular N□H···O Hydrogen Bonds in Pyrrolyl Derivatives of Indane-1,3-Dione—Experimental and Theoretical Study. *J. Phys. Org. Chem.* **2009**, *22* (12), 1178−1187.
(40) Institute of Solid State Physics. *The Computations Were Performed on Latvian SuperCluster (LaSC)*; University of Latvia, 2023 The computations were performed on Latvian SuperCluster (LaSC), located in the Institute of Solid State Physics, University of Latvia.
(41) O'Boyle, N. M.; Banck, M.; James, C. A.; Morley, C.; Vandermeersch, T.; Hutchison, G. R. Open Babel: An Open Chemical Toolbox. *J. Cheminform.* **2011**, *3* (1), 33.
(42) Frisch, M. J.; Trucks, G. W.; Schlegel, H. B.; Scuseria, G. E.; Robb, M. A.; Cheeseman, J. R.; Scalmani, G.; Barone, V.; Petersson, G. A.; Nakatsuji, H.; Li, X.; Caricato, M.; Marenich, A. V.; Bloino, J.; Janesko, B. G.; Gomperts, R.; Mennucci, B.; Hratchian, H. P.; Ortiz, J. V.; Izmaylov, A. F.; Sonnenberg, J. L.; Williams; Ding, F.; Lipparini, F.; Egidi, F.; Goings, J.; Peng, B.; Petrone, A.; Henderson, T.; Ranasinghe, D.; Zakrzewski, V. G.; Gao, J.; Rega, N.; Zheng, G.; Liang, W.; Hada, M.; Ehara, M.; Toyota, K.; Fukuda, R.; Hasegawa, J.; Ishida, M.; Nakajima, T.; Honda, Y.; Kitao, O.; Nakai, H.; Vreven, T.; Throssell, K.; Montgomery, J. A., Jr.; Peralta, J. E.; Ogliaro, F.; Bearpark, M. J.; Heyd, J. J.; Brothers, E. N.; Kudin, K. N.; Staroverov, V. N.; Keith, T. A.; Kobayashi, R.; Normand, J.; Raghavachari, K.; Rendell, A. P.; Burant, J. C.; Iyengar, S. S.; Tomasi, J.; Cossi, M.; Millam, J. M.; Klene, M.; Adamo, C.; Cammi, R.; Ochterski, J. W.; Martin, R. L.; Morokuma, K.; Farkas, O.; Foresman, J. B.; Fox, D. J. *Gaussian 16*, revision C.01; Gaussian, Inc.: Wallington, CT, 2016.
(43) Yu, H. S.; He, X.; Li, S. L.; Truhlar, D. G. MN15: A Kohn−Sham Global-Hybrid Exchange−Correlation Density Functional with Broad Accuracy for Multi-Reference and Single-Reference Systems and Noncovalent Interactions. *Chem. Sci.* **2016**, *7* (8), 5032−5051.
(44) Kozuch, S.; Martin, J. M. L. DSD-PBEP86: In Search of the Best Double-Hybrid DFT with Spin-Component Scaled MP2 and Dispersion Corrections. *Phys. Chem. Chem. Phys.* **2011**, *13* (45), 20104.
(45) Mardirossian, N.; Head-Gordon, M. How Accurate Are the Minnesota Density Functionals for Noncovalent Interactions, Isomerization Energies, Thermochemistry, and Barrier Heights Involving Molecules Composed of Main-Group Elements? *J. Chem. Theory Comput.* **2016**, *12* (9), 4303−4325.
(46) Goerigk, L.; Hansen, A.; Bauer, C.; Ehrlich, S.; Najibi, A.; Grimme, S. A Look at the Density Functional Theory Zoo with the Advanced GMTKN55 Database for General Main Group Thermochemistry, Kinetics and Noncovalent Interactions. *Phys. Chem. Chem. Phys.* **2017**, *19* (48), 32184−32215.
(47) Santos, P. F.; Reis, L. V.; Almeida, P.; Lynch, D. E. Crystal Structures of a Benzoselenazole-Derived Squarylium Cyanine Dye and Three Derivatives Substituted at the Central Squaric Ring. *CrystEngComm* **2011**, *13* (5), 1333−1338.
(48) Andersen, N. H.; Neidigh, J. W.; Harris, S. M.; Lee, G. M.; Liu, Z.; Tong, H. Extracting Information from the Temperature Gradients of Polypeptide NH Chemical Shifts. 1. The Importance of Conformational Averaging. *J. Am. Chem. Soc.* **1997**, *119*, 8547−8561.
(49) Cierpicki, T.; Otlewski, J. Amide Proton Temperature Coefficients as Hydrogen Bond Indicators in Proteins. *J. Biomol. NMR* **2001**, *21* (3), 249−261.
(50) Gottlieb, H. E.; Kotlyar, V.; Nudelman, A. NMR Chemical Shifts of Common Laboratory Solvents as Trace Impurities. *J. Org. Chem.* **1997**, *62* (21), 7512−7515.

https://doi.org/10.1021/acsomega.3c07005
ACS Omega 2023, 8, 40960−40971